

# Generic magnetic field dependence of thermal conductivity in effective spin-1/2 magnetic insulators via hybridization of acoustic phonons and spin-flip excitations

Christopher A. Pocs<sup>†,1</sup>, Jie King,<sup>2</sup> Eun Sang Choi,<sup>3</sup> Athena S. Sefat,<sup>2</sup> Michael Hermele,<sup>1,4</sup> and Minhyea Lee<sup>1</sup>

<sup>1</sup>*Department of Physics, University of Colorado, Boulder, Colorado 80309, USA*

<sup>2</sup>*Materials Science and Technology Division, Oak Ridge National Laboratory, Oak Ridge, Tennessee 37831, USA*

<sup>3</sup>*National High Magnetic Field Laboratory, Tallahassee, Florida, USA*

<sup>4</sup>*Center for Theory of Quantum Matter, University of Colorado, Boulder, Colorado 80309, USA*

(Dated: January 4, 2024)

It is common to observe a notable non-monotonic dependence of thermal conductivity on applied magnetic field in magnetic insulators. This prevalent behavior prompts the need for an explanation involving components present in a wide range of systems. We report the field-dependence of thermal conductivity in the well-characterized effective spin-1/2 paramagnetic insulator CsYbSe<sub>2</sub>. Along with the data, we propose that the observed non-monotonic field dependence results from the hybridization of acoustic phonons with spin-flip excitations across the Zeeman gap, where the magnetoelastic coupling arises via modulation of the magnetic  $g$ -tensor by local strain. This hypothesis aligns with a simple theoretical model that qualitatively reproduces key features of the data on CsYbSe<sub>2</sub>. Our results provide a starting point to understand the magnetic field dependence of thermal conductivity in a broad spectrum of magnetic insulators.

Thanks to its exclusive sensitivity to itinerant excitations, thermal conductivity is one of the most valuable probes for examining magnetic insulators and for characterizing the magnetic ground state [1–5]. The magnetic field ( $H$ ) dependence of thermal transport has been argued to be a signature of unconventional spin excitations [6–12]. However, even though phonon excitations of the crystalline lattice are the dominant heat carriers, much of our understanding relies on viewing them in a subsidiary role. When phonons are not entirely neglected in studying the field-dependence of thermal conductivity, one typically considers a thermal current of phonons scattering off spin excitations. While such perspectives can be useful, they can also be oversimplifications that lead us to miss essential physics.

A case in point is the non-monotonic field dependence of thermal conductivity ( $\kappa$ ) that has been observed in the paramagnetic states of several effective spin-1/2 magnetic insulators. Namely, (1)  $\kappa(H)$  first decreases to a minimum at  $H = H_{\min}$  followed by an increase and (2)  $H_{\min}$  moves toward large values with increasing temperature. Systems showing this behavior include Cu<sub>3</sub>VO<sub>7</sub>(OH)<sub>2</sub>·H<sub>2</sub>O [7], YbTiO<sub>7</sub> [8], Cd-kapellasite [10], gadolinium gallium garnet [13], and  $\alpha$ -RuCl<sub>3</sub> above its ordering temperature [14]. Explaining this phenomenology in terms of spin-phonon scattering alone is not plausible, without invoking unusual responses of the spin sector to applied field that seem unlikely to be present across such a wide range of systems. Instead, a generic explanation is called for that involves only common ingredients, and that treats phonon and spin excitations on equal footing.

Here, we propose such an explanation via our study of the well-characterized Kramers pseudospin-1/2 Yb-based triangular lattice CsYbSe<sub>2</sub>, where we observed the non-monotonic field dependence of  $\kappa$  described above. We propose that the heat conduction under field is enabled by the hybridized quasiparticles formed from acoustic phonons and spin-flip excitations (SFEs)

across the Zeeman gap, and hypothesize that the resulting hybridized excitations are responsible for the non-monotonic  $\kappa(H)$ . This aligns with a highly simplified theoretical model that qualitatively reproduces key features of the experimental data. The two main ingredients of our model, namely (1) single-ion Zeeman splitting and associated SFEs and (2) magnetoelastic (ME) coupling that mediates phonon-SFE hybridization, are common in magnetic insulators. Therefore, our results offer a starting point to understand the non-monotonic field-dependence of  $\kappa$  observed in a range of other systems. We remark that previous works have studied hybridization between different types of magnetic excitations and phonons [15–19], although their focus has been on spectroscopic probes, and we are not aware of prior studies considering the effects on transport.

The Yb-based triangular-lattice compound CsYbSe<sub>2</sub> has space group  $P6_3/mmc$  and consists of layers of edge-sharing YbSe<sub>6</sub> octahedra separated by Cs<sup>3+</sup> ions as shown in Fig. 1a [21]. Yb<sup>3+</sup> carries a  $J = 7/2$  magnetic moment, which is split into four doubly degenerate crystal electric field (CEF) levels at zero field. CsYbSe<sub>2</sub> shows no long-range order down to 0.3 K at zero field, with signs of field-induced local correlations below 1 K [22]. Single-ion CEF parameters have been determined in [20], allowing for calculations of the magnetization within the Weiss-mean field approximation [Fig. 1b], which agree well with the magnetization data up to  $\mu_0 H = 7$  T. The CEF energy spectrum under field was also obtained and shown in Fig. 1c, where the Kramers doublets are split via the Zeeman effect under applied field. When the temperature ( $T$ ) is lowered below the first excitation energy gap ( $E_1 - E_0 \simeq 13$  meV), restriction of the dynamics to the ground doublet justifies the use of a pseudospin-1/2 model.

The first order Zeeman splitting of the ground doublet is encoded in the Hamiltonian  $\mathcal{H}_Z = \mu_B \mu_0 (g_z H_z \hat{S}^z +$

arXiv:2401.01407v1 [cond-mat.str-el] 2 Jan 2024

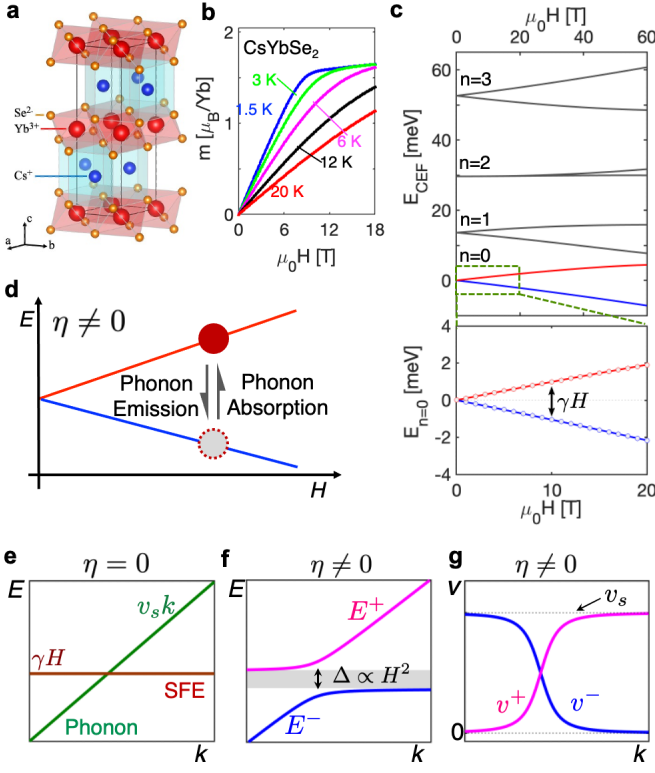


FIG. 1. **a** Crystal structure of CsYbSe<sub>2</sub>: Yb<sup>3+</sup> (red) forms triangular nets within the *ab* plane, formed by edge-sharing YbSe<sub>6</sub> octahedra. **b** Calculated single-ion magnetization within Weiss mean-field approximation [20]. **c** Field dependent crystal electric field energy spectrum calculated with the parameters in [20], where linear splitting of the ground state doublets is shown. The ground state Zeeman gap is  $\gamma H$  with  $\gamma = 0.22$  meV/T. **d** Schematic illustration of the processes leading to hybridization of phonons and SFEs, where a SFE decays (is created) by emitting (absorbing) a phonon. **e** Schematic sketch of the dispersion relation with no ME coupling ( $\eta = 0$ ). A flat band of SFEs has energy  $\gamma H$ , independent of wave vector  $k$ , while an acoustic phonon has a linear dispersion with slope  $v_s$ . **f** Schematic dispersion relation in the presence of non-zero ME coupling ( $\eta \neq 0$ ), where hybridization leads to an avoided crossing and the opening of a gap between upper and lower branches of hybrid SFE-phonon excitations. **g** Group velocities  $v_{\pm} = \frac{dE_{\pm}}{dk}$ , derived from the dispersion of the hybridized excitations.

$g_{\perp} H_x \hat{S}^x + g_{\perp} H_y \hat{S}^y$ ), where  $\hat{S}^i$  are the pseudospin-1/2 operators and  $g_z$  and  $g_{\perp}$  the components of the anisotropic  $g$ -factor [20]. We always consider field applied along the  $x$ -axis (within the crystalline *ab*-plane), so the Zeeman gap of the ground doublet is  $\gamma H = g\mu_B\mu_0 H$ , where  $g \equiv g_{\perp} = 2g_J|(0_{\pm}|\hat{J}_x|0_{\mp})|$ . Here  $\hat{J}_x$  is the angular momentum operator in the direction of the applied field,  $|0_{\pm}\rangle$  are the energy eigenstates of the doublet under applied  $z$ -axis field, and  $g_J$  is the Landé  $g$ -factor for the Yb<sup>3+</sup> ion.

SFEs are excitations across the Zeeman gap, where a single pseudospin is flipped from its  $S^x = -1/2$  ground

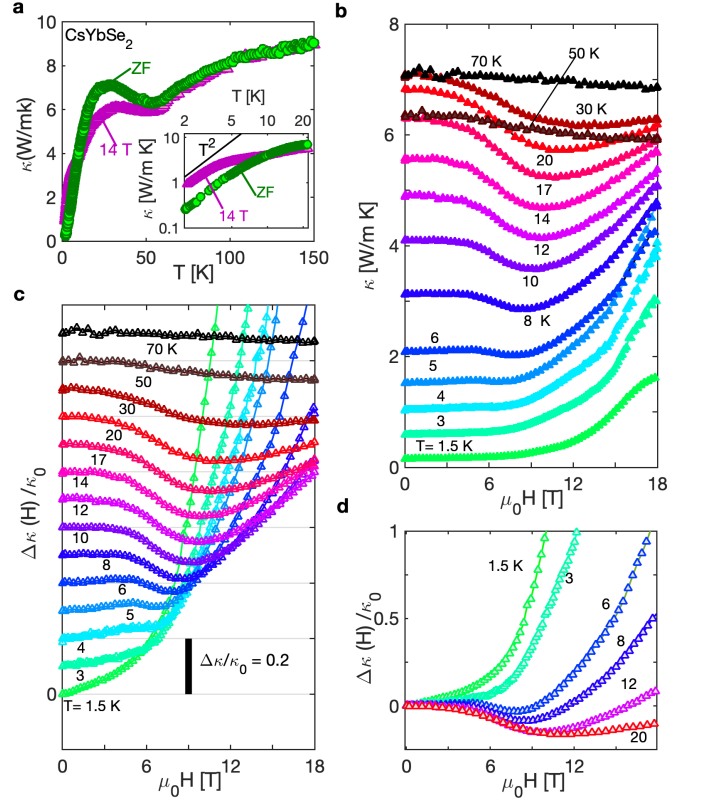


FIG. 2. **a** Temperature dependence of thermal conductivity  $\kappa$ , where  $\nabla T \parallel ab$  at zero field and  $\mu_0 H = 14$  T, with field aligned to the heat current. Inset shows the magnified view for  $T < 20$  K, where  $T^2$ -like behavior can be seen at lower temperatures. **b** Magnetic field dependence of  $\kappa$  is shown at various temperatures. At low temperature  $T < 5$  K,  $\kappa(H)$  exhibits little field-dependence at small field, followed by a rapid rise as the field is increased through  $\mu_0 H \approx 9$  T. Starting above  $T = 5$  K, a shallow minimum of  $\kappa(H)$  appears at  $H = H_{\min}$ , where  $H_{\min}$  increases with temperature. **c** Fractional thermal conductivity  $\Delta\kappa(H)/\kappa_0$ , where  $\kappa_0 = \kappa(\mu_0 H = 0)$ , is plotted as a function of  $H$  at various temperatures. The data are plotted with offset for clarity. **d** Fractional thermal conductivity at selected temperatures as indicated.

state to the  $S^x = +1/2$  excited state. Without hybridization of SFEs and phonons, there is a flat band of non-propagating SFEs (Fig. 1e). Hybridization modifies the dispersion of SFEs and phonons as shown schematically in Fig. 1f, leading to two branches of mixed excitations with non-zero group velocities (Fig. 1g).

The CsYbSe<sub>2</sub> system is particularly well-suited to explore the hybridization of acoustic phonons and SFEs: (1) The CEF gap between the ground and first excited doublets ( $\Delta_{10}$ ) is large enough ( $\sim 13$  meV) to provide a large  $T$  range where the effective spin-1/2 approximation is valid. (2) The small exchange energy ( $J_{\text{ex}} \approx 0.4$  meV) combined with geometric frustration prevents long-range magnetic order [20, 22], leading to a wide paramagnetic regime where spin-spin exchange interactions may be ne-

glected to a first approximation.

Fig. 2 displays the thermal conductivity of CsYbSe<sub>2</sub> as a function of temperature  $1.5\text{ K} < T < 150\text{ K}$  and field up to  $\mu_0 H = 18\text{ T}$ , within the paramagnetic state, where the temperature gradient and field are parallel and within the  $ab$  plane. For  $T < 50\text{ K}$ , the  $T$ -dependence of  $\kappa$  is affected by field, where  $\mu_0 H = 14\text{ T}$  enhances (suppresses)  $\kappa$  at low (high) temperatures as shown in Fig. 2a. The non-monotonic field dependence is clarified by plotting  $\kappa$  versus  $H$  at several values of  $T$  in Fig. 2b. When  $T < 5\text{ K}$ ,  $\kappa(H)$  exhibits weak field-dependence as  $H$  is first increased from zero, then rapidly increases upon further increasing  $H$ . As  $T$  increases above  $5\text{ K}$ ,  $\kappa(H)$  shows a decrease with increasing  $H$  until reaching a pronounced minimum at  $H = H_{\min}$ . The field  $H_{\min}$  moves to large values as  $T$  increases, eventually becoming hard to locate as the field-dependence is diminished. Fig. 2c and d show the fractional thermal conductivity  $\Delta\kappa(H)/\kappa_0 \equiv (\kappa(H) - \kappa_0)/\kappa_0$ , where  $\kappa_0$  is the value at zero field at a given  $T$ . This quantity is plotted with a constant offset along the  $y$ -axis to highlight the monotonic increase of  $H_{\min}$  with  $T$ .

To explain the  $\kappa(H)$  data of CsYbSe<sub>2</sub>, we need to consider a coupling between phonons and magnetic excitations. Recalling that the CEF effect arises from electrostatic interactions between a single magnetic ion and its surrounding ligands, small lattice distortions can create a modulation of the characteristic magnetic energy scales, leading to ME coupling. For example, varying the distortion of YbSe<sub>6</sub> octahedra will change the anisotropy of the  $g$ -tensor  $g_z/g_{\perp}$ . At sufficiently low  $T$  when only the ground doublet is occupied, the most general linear ME coupling arising from local lattice distortions is  $\mathcal{H}_{ME} = \mu_0\mu_B \sum_{i,j} H_i \delta g_{ij} \hat{S}^j$ . That is, ME coupling enters via a modulation of the  $g$ -tensor  $\delta g_{ij}$ . For small lattice distortions each component of  $\delta g$  is a linear combination of components of the symmetric strain tensor  $\epsilon_{ij} = \partial_i u_j + \partial_j u_i$ , where  $u_i$  is the displacement field. We note that lattice distortions do not couple to the pseudospin in the limit of zero field, where time reversal symmetry holds and Kramers theorem prevents any splitting of the ground doublet. This contrasts with non-Kramers doublet systems such as TmVO<sub>4</sub>, where the ME coupling remains non-zero in vanishing applied field [15].

The most dramatic consequence of this ME coupling turns out to be the hybridization of SFEs and phonons, arising from terms corresponding to the emission/absorption processes illustrated in Fig. 1c. Here we introduce a highly simplified effective model designed to capture the essential qualitative physics of hybridization as manifested in thermal conductivity. Our model can be motivated by a more microscopic treatment sketched in the Methods Section. The SFEs are treated as bosons within a standard spin wave approximation, and we focus on only a single polarization of acoustic phonon. The energies  $E_{\pm}(k)$  of the two branches of hybridized excita-

tions are the eigenvalues of the matrix

$$\mathcal{H}(k) = \begin{pmatrix} \hbar v_s k & \sqrt{\eta \hbar v_s k} \gamma H \\ \sqrt{\eta \hbar v_s k} \gamma H & \gamma H \end{pmatrix}, \quad (1)$$

where  $v_s$  is the sound velocity and  $\gamma = g\mu_B\mu_0 = 0.22\text{ meV/T}$  as shown in Fig. 1c. From specific heat in zero field (data not shown), we obtained  $\hbar v_s = 12.97\text{ meV \AA}$  equivalent to  $2.80 \times 10^3\text{ m/sec}$  and also the Debye energy  $\hbar\omega_D = 7.1\text{ meV}$ . The off-diagonal matrix elements arise from  $\mathcal{H}_{ME}$  with ME coupling strength parametrized by  $\eta$ . The  $\sqrt{k}$ -dependence matches the scaling of off-diagonal matrix elements within the microscopic treatment illustrated in the Methods Section. Here, we neglect any angular dependence and assume that the hybridized excitations have a spherically symmetric dispersion. The off-diagonal term in Eq. 1 makes it transparent that applied field simultaneously tunes the Zeeman gap  $\gamma H$  and the strength of ME coupling.

The energies of hybridized quasiparticles take the form

$$E_{\pm}(k) = \left( \frac{E_0 + \gamma H}{2} \right) \pm \sqrt{\left( \frac{E_0 - \gamma H}{2} \right)^2 + \eta E_0 \gamma^2 H^2}, \quad (2)$$

where  $E_0 = \hbar v_s k$ . The dispersion of  $E_{\pm}$  as a function of wavevector  $k$  is plotted in Fig. 3a-c for applied fields  $\mu_0 H = 4, 8, \text{ and } 16\text{ T}$ , respectively. The Debye energy  $E_D$  is marked as a dotted line. The lower branch  $E_-(k)$  increases monotonically from zero to  $\gamma H - \eta(\gamma H)^2$  as  $k \rightarrow \infty$ , while the upper branch  $E_+(k)$  starts at  $E_+(k=0) = \gamma H$  and monotonically increases. The size of the gap ( $\Delta$ ) between the two branches thus takes the simple form  $\Delta = \eta(\gamma H)^2$  when including states with arbitrarily large values of  $k$ . The gap size increases modestly upon imposing the momentum cutoff  $k < \pi/a$  as illustrated by the gray shading in Fig. 3; here,  $a = 4.41607\text{ \AA}$  is the  $ab$ -plane lattice constant. Note that the lower branch dispersion becomes flat with  $E_-(k) = 0$  when  $\eta = (\gamma H)^{-1}$ , signaling an instability reached either at large ME coupling or strong applied field, beyond which the model will not be valid. We thus always take  $\eta < (\gamma H)^{-1}$ , where  $E_-(k)$  is non-zero and remains real. Fig. 3d displays a magnified view in the low-energy region: the slope (*i.e.* group velocity) at  $k = 0$  decreases monotonically with increasing field. This is important for determining the high field behavior as discussed below.

Thermal conductivity is computed within a Debye-Callaway model [23] using the above hybridized quasiparticle spectra:

$$\begin{aligned} \kappa(T, H) &= \frac{\tau}{3} \sum_{\sigma=\pm} \int \frac{d\mathbf{k}^3}{(2\pi)^3} c(E_{\sigma}(k)) v_{\sigma}^2(k), \quad (3) \\ &= \frac{\tau}{3} \int_0^{\infty} dE c(E) v^2(E) g(E). \quad (4) \end{aligned}$$

Here,  $v_{\pm} = (1/\hbar)dE_{\pm}/dk$  and  $c(E) = Edn_B/dT$  is the specific heat of a single bosonic mode, with  $n_B(T)$  the standard Bose occupation function. The scattering time

$\tau$  normally has both temperature and  $k$  dependence [23]. However, we always take  $\tau$  to be  $k$ -independent to focus on the effect of hybridization. In Eq. 3, we impose the momentum cutoff  $k < \pi/a$ . We rewrite  $\kappa$  as an energy integral in Eq. (4), via the density of states  $g(E)$  of the hybridized excitations. In Fig. 3e, the integrand of Eq. (4) is plotted for a few values of  $H$  at fixed  $T = 6$  K. The upper and lower branches are clearly visible as two separate peaks separated by the gap (within which the function vanishes). As the field is increased from zero, the contribution of the upper branch decreases as spectral weight moves to higher energy, while that of the lower branch increases with field.

The measured  $\Delta\kappa/\kappa_0$  of CsYbSe<sub>2</sub> and the calculated result are shown Fig. 4a and b, respectively, as a function of applied field. In the calculation, we use  $\eta = 0.13$  meV<sup>-1</sup>, and take  $\tau$  to be independent of magnetic field, as appropriate for non-magnetic scattering. The temperature dependence of  $\tau$  plays no role, as it cancels out in the fractional thermal conductivity. Our minimal model qualitatively captures the essential characteristics of the data: non-monotonic field-dependence of  $\kappa$  observed for  $T > 5$  K, as well as the movement of  $H_{\min}$  to larger values with increasing  $T$ . However, there are discrepancies between the data and the model that we return to below.

We now discuss how to understand the non-monotonic field dependence of  $\kappa$  in terms of the hybridized phonon-SFEs based on simple arguments, independent of the details of our model. We assume relatively weak ME coupling such that  $\eta\gamma H < c$ , where  $c < 1$  is an arbitrary dimensionless constant chosen not too close to 1; a simple perturbation theory argument shows that this condition prevents this hybridization from modifying the dispersion too strongly at large wave vector.

First, we consider the low- $H$  regime where  $\gamma H \ll k_B T$ . In general, excitations contribute more strongly to  $\kappa$  when their energy density changes rapidly with temperature. This is quantified by the heat capacity  $c(E)$  of bosonic excitations (inset of Fig. 3e), which appears as a weighting factor in Eq. 4.  $c(E)$  is only weakly  $T$ -dependent for  $E \lesssim k_B T$  and decreases exponentially for  $E \gtrsim k_B T$ . As in Fig. 3a, upon increasing  $H$ , opening the gap between upper and low branches pushes spectral weight in the upper (lower) branch to higher (lower) energies. The effect of this on  $\kappa$  is dominated by the upper branch, where  $c(E)$  falls off rapidly with energy, and pushing spectral weight to higher energies leads to a decrease in  $\kappa$ , as can be seen in Fig. 3d. On the contrary, for the energy scales in the lower branch,  $c(E)$  only depends on weakly on energy and hence the shift in spectral weight does not strongly affect  $\kappa$ .

Turning to the high-field  $\gamma H \gg k_B T$  regime, only lower-branch states with  $k \approx 0$  are appreciably thermally occupied, and the lower branch gives the dominant contribution to  $\kappa$  and hence its field-dependence. Moreover, we can approximate the linear dispersion  $E_-(k) \approx \hbar v_{\text{eff}} k$  near  $k = 0$  (Fig. 3d). As  $H$  increases, level repulsion bends the  $k \approx 0$  lower-branch dispersion downward as il-

lustrated in Fig. 3b, resulting in  $v_{\text{eff}}$  that decreases with increasing field. Within our model, the lower-branch velocity at  $k = 0$  is indeed given by  $v_- = v_s - v_s \eta \gamma H$ . Examining Eq. 4, one might naïvely conclude that  $\kappa$  should decrease as  $v_{\text{eff}}$  decreases, given the factor of  $v(E)^2 \approx v_{\text{eff}}^2$  in the integrand. However, the density of states for a linearly dispersing mode of velocity  $v_{\text{eff}}$  is  $g(E) = E^2/2\pi^2 \hbar^3 v_{\text{eff}}^3$ , so in fact  $\kappa \propto v_{\text{eff}}^{-1}$  in the high-field regime, and  $\kappa$  thus increases with increasing field, which is well-captured in Fig. 4.

Finally, we discuss the discrepancies between the  $\Delta\kappa/\kappa_0$  data and the calculation shown in Fig. 4a and b. As compared to the calculation, the data shows a more pronounced increase of  $\Delta\kappa/\kappa_0$  at large applied field, and lacks the minimum in  $\Delta\kappa/\kappa_0(H)$  for  $T < 5$  K. These differences prompt us to consider two simple improvements to our model. First, SFEs are subject to a hard-core repulsive interaction that prevents two excitations from occupying the same lattice site, an effect that becomes more important with increasing temperature due to thermally excited SFEs. In our linear spin-wave treatment of the SFEs, the excitations are represented by bosonic particles that can have arbitrarily high occupation number on a given lattice site. The hard-core repulsive interaction of SFEs can be restored at a mean-field level via temperature-dependent ME coupling  $\eta = \eta(T)$ , as described in the Methods Section. The coupling  $\eta(T)$  is expected to decrease with increasing  $T$  due to increased thermal occupation of SFEs. In Fig. 4c, we employ an empirical monotonically decreasing form for  $\eta(T)$ , as shown in the inset. This correction turns out to have only a small effect on  $\Delta\kappa/\kappa_0(H)$  except at the lowest temperatures ( $T = 1.5$  K), where it results in a more pronounced increase at large field.

Second, we expect phonons to scatter off of fluctuating paramagnetic moments, with a scattering rate proportional to the effective density of the magnetic scattering centers  $n_{\text{mag}}$ , which is estimated as  $n_{\text{mag}}(T, H) = \frac{\Delta M(T, H)}{M_S} = \frac{M(T, H) - M_S}{M_S}$ , where  $M_S$  is the saturated magnetization as treated in [24]. Such scattering is thus suppressed with increasing applied field, as the magnetization approaches saturation. This can be incorporated in a simple manner by replacing the scattering rate with  $\tau^{-1}(H) = \tau_0^{-1}(1 + \alpha n_{\text{mag}}(H))$  at a given  $T$ , where  $\alpha$  depends on  $T$  and measures the relative strength of magnetic to non-magnetic scattering. Using the field dependence of magnetization calculated in the Weiss mean-field approximation [20] shown in Fig. 1b, we replace the  $\tau$  in Eq. (3) with  $\tau(H)$  above to obtain  $\Delta\kappa/\kappa_0$  as a function of  $H$  using the same  $\eta(T)$  in Fig. 4c and  $\alpha(T)$  displayed in Fig. 4d. We find this correction has a much larger effect: a strong rise in  $\kappa$  at large field and significantly reduced size of the minimum  $\Delta\kappa/\kappa_0$  at  $H_{\min}$ , which further increases the qualitative agreement of the model with the data. However, these corrections do not remove completely the model's pronounced minimum in  $\kappa$  at low  $T$  and small applied fields. Needless to say, our minimal model does not account for material-specific de-

tails such as spin-spin exchange interactions, proximity to magnetic order, multiple phonon polarizations, and anisotropy in the unperturbed phonon dispersion and ME coupling, all of which may play a role. We also expect that microscopic treatments of scattering processes of the hybridized quasiparticles will bring the model closer to the observed  $\Delta\kappa/\kappa_0$ .

In summary, our study demonstrated that the field dependence of thermal conductivity in CsYbSe<sub>2</sub> can be attributed to heat transport by hybridized quasiparticles formed from acoustic phonons and SFEs. Our highly simplified model qualitatively captures (1) the initial decrease of  $\kappa$  under applied magnetic field to a minimum at  $H = H_{\min}$ , followed by an increase at higher fields and (2) the monotonic increase of  $H_{\min}$  with  $T$ . Including an  $H$ -dependent relaxation time improves the qualitative agreement between the model and the data. The key ingredients of our model are Zeeman splitting, acoustic phonons, and weak ME coupling via modulation of the magnetic  $g$ -tensor by local strain, all of which are found in many systems. We thus expect that phonon-SFE hybridization will be a useful starting point to understand the field dependence of thermal transport in a wide range of magnetic insulators.

## ACKNOWLEDGMENTS

We thank Y. Matsuda and Y. Kasahara for helpful discussions. Work at University of Colorado Boulder was supported by the U.S. Department of Energy, Office of Science, Basic Energy Sciences (BES) under Award No. DE-SC0021377 (experimental work by C.A.P. and M.L.) and Award No. DE-SC0014415 (theoretical work by M.H.). Work at Oak Ridge National Laboratory (ORNL) was supported by the U.S. Department of Energy, Office of Science, Basic Energy Sciences, Materials Sciences and Engineering Division. A portion of this work was performed at the National High Magnetic Field Laboratory, which is supported by National Science Foundation Cooperative Agreement No. DMR-1644779, the State of Florida, and the U.S. Department of Energy.

## Appendix: Methods

Here we sketch a more microscopic theoretical treatment of the problem of coupled acoustic phonons and SFEs, which motivates the simplified effective model described in the main text. We treat the acoustic phonons

as excitations of a continuous elastic medium with displacement field  $u_i(\mathbf{r})$  and symmetric stress tensor  $\epsilon_{ij} = \partial_i u_j + \partial_j u_i$ . Spin-1/2 spins  $\hat{S}_\mathbf{r}^i$  lie on the sites of a Bravais lattice, and the ME coupling takes the form  $\mathcal{H}_{ME} = \sum_{\mathbf{r}} \mathcal{H}_{ME}(\mathbf{r})$ , where the sum is over lattice sites and  $\mathcal{H}_{ME}(\mathbf{r}) = \mu_0 \mu_B H_x \delta g_{xi}(\mathbf{r}) \hat{S}_\mathbf{r}^i$  as described in the main text. (In this Appendix, sums over repeated indices are implied.) We drop the  $i = x$  term as it does not lead to hybridization of phonons and SFEs, and the remaining terms can be written  $\mathcal{H}_{ME}(\mathbf{r}) = \mu_0 \mu_B H_x [\Lambda_{ij} \epsilon_{ij} \hat{S}_\mathbf{r}^+ + \text{H.c.}]$ , where  $\Lambda_{ij}$  is a complex matrix of coupling constants parametrizing the ME coupling and the spin raising operators are defined by  $\hat{S}_\mathbf{r}^+ \equiv \hat{S}_\mathbf{r}^y + i\hat{S}_\mathbf{r}^z$  (also  $S_\mathbf{r}^- = (S_\mathbf{r}^+)^\dagger$  for spin lowering operators). These spin raising/lowering operators are defined to raise/lower  $\hat{S}_\mathbf{r}^x$ , corresponding to the direction of applied field.

To study the effect of  $\mathcal{H}_{ME}$ , we go to momentum space. The Fourier transform of the displacement field is

$$u_i(\mathbf{r}) = \sum_{\mathbf{k}, \lambda} \sqrt{\frac{\hbar}{2V\rho\omega_\lambda(\mathbf{k})}} e^{i\mathbf{k}\cdot\mathbf{r}} \hat{e}_{\lambda i}(\mathbf{k}) [a_{\mathbf{k}\lambda} + a_{\mathbf{k}\lambda}^\dagger], \quad (\text{A.1})$$

where  $V$  is the volume,  $\rho$  the mass density of the crystal, and  $\lambda$  labels the three phonon polarizations with frequencies  $\omega_\lambda(\mathbf{k}) = v_\lambda k$ , polarization vectors  $\hat{e}_\lambda(\mathbf{k})$ , and creation operators  $a_{\mathbf{k}\lambda}^\dagger$ . Because we treat the lattice as a continuous medium, the magnitude of the wave vector  $\mathbf{k}$  is unrestricted in the sum. For the spin operators, we define the Fourier transform by

$$S_\mathbf{r}^+ = \frac{1}{\sqrt{N}} \sum_{\mathbf{k} \in \text{BZ}} e^{-i\mathbf{k}\cdot\mathbf{r}} S_\mathbf{k}^+, \quad (\text{A.2})$$

where  $N$  is the number of lattice sites and the wave vector sum is restricted to the first Brillouin zone.

To make a linear spin-wave approximation, we introduce Holstein-Primakoff bosons with creation operators  $b_\mathbf{r}^\dagger$  by writing  $S_\mathbf{r}^+ = b_\mathbf{r}^\dagger \sqrt{1 - b_\mathbf{r}^\dagger b_\mathbf{r}}$ . We note the form of Eq. (A.2) is chosen so that if we ignore the square root and thus replace  $S_\mathbf{r}^+$  by  $b_\mathbf{r}^\dagger$  and  $S_\mathbf{k}^+$  by  $b_\mathbf{k}^\dagger$ , the momentum space creation/annihilation operators satisfy canonical commutation relations. Simply dropping the square root neglects the hard-core nature of the Holstein-Primakoff bosons, but we can restore this effect at a mean-field level by replacing  $S_\mathbf{r}^+ \rightarrow \sqrt{1 - \bar{n}} b_\mathbf{r}^\dagger$ , where  $\bar{n} = \langle b_\mathbf{r}^\dagger b_\mathbf{r} \rangle$ .

Plugging the Fourier transforms into  $\mathcal{H}_{ME}$ , keeping only hybridization terms proportional to  $a_{\mathbf{k}\lambda}^\dagger b_\mathbf{k}$  (or the Hermitian conjugate), and dropping contributions from higher energy phonons outside the first Brillouin zone, we have

$$\mathcal{H}_{ME} = \sqrt{1 - \bar{n}} \mu_0 \mu_B H_x \sum_{\mathbf{k} \in \text{BZ}} \sum_{\lambda} \left\{ \sqrt{\frac{\hbar}{2v_{uc}\rho\omega_\lambda(\mathbf{k})}} \Lambda_{ij} [ik_i \hat{e}_{\lambda j}(\mathbf{k}) + ik_j \hat{e}_{\lambda i}(\mathbf{k})] a_{\mathbf{k}\lambda} b_\mathbf{k}^\dagger + \text{H.c.} \right\}. \quad (\text{A.3})$$

Here  $v_{uc}$  is the volume of a crystalline unit cell. We note that the matrix elements of this Hamiltonian are proportional to  $\sqrt{k}$ , which comes from the factors of  $k_i/\sqrt{\omega_\lambda(\mathbf{k})}$ ; this motivates the  $\sqrt{k}$ -dependence of the off-diagonal matrix elements in the effective model of the main text. Moreover, the effect of the mean-field correction  $\sqrt{1-\bar{n}}$  is to renormalize the overall strength of the ME coupling, giving a temperature-dependent coupling that goes down

as thermal occupation of SFEs increases.

Finally, we remark that it would be possible to compute  $\kappa$  along the same lines as in the main text using the ME coupling of Eq. A.3 and including all three phonon polarizations. While this may be valuable to explore in future work, it is important to emphasize that this introduces additional adjustable parameters associated with couplings to different phonon polarizations, significantly increasing the complexity of the model.

- 
- [1] J. Wen, S.-L. Yu, S. Li, W. Yu, and J.-X. Li, *npj Quantum Materials* **4**, 12 (2019).
- [2] A. V. Sologubenko, K. Giannó, H. R. Ott, U. Ammerahl, and A. Revcolevschi, *Phys. Rev. Lett.* **84**, 2714 (2000).
- [3] C. Hess, C. Baumann, U. Ammerahl, B. Büchner, F. Heidrich-Meisner, W. Brenig, and A. Revcolevschi, *Phys. Rev. B* **64**, 184305 (2001).
- [4] S. Y. Li, L. Taillefer, C. H. Wang, and X. H. Chen, *Phys. Rev. Lett.* **95**, 156603 (2005).
- [5] L. Savary and L. Balents, *Rep. Prog. Phys.* **80**, 016502 (2016).
- [6] M. Hirschberger, J. W. Krizan, R. J. Cava, and N. P. Ong, *Science* **348**, 106 (2015).
- [7] D. Watanabe, K. Sugii, M. Shimozawa, Y. Suzuki, T. Yajima, H. Ishikawa, Z. Hiroi, T. Shibauchi, Y. Matsuda, and M. Yamashita, *Proceedings of the National Academy of Sciences* **113**, 8653 (2016).
- [8] Y. Tokiwa, T. Yamashita, M. Udagawa, S. Kittaka, T. Sakakibara, D. Terazawa, Y. Shimoyama, T. Terashima, Y. Yasui, T. Shibauchi, and Y. Matsuda, *Nat. Commun.* **7**, 10807 (2016).
- [9] Y. Kasahara, T. Ohnishi, Y. Mizukami, O. Tanaka, S. Ma, K. Sugii, N. Kurita, H. Tanaka, J. Nasu, Y. Motome, T. Shibauchi, and Y. Matsuda, *Nature* **559**, 227 (2018).
- [10] M. Akazawa, M. Shimozawa, S. Kittaka, T. Sakakibara, R. Okuma, Z. Hiroi, H.-Y. Lee, N. Kawashima, J. H. Han, and M. Yamashita, *Phys. Rev. X* **10**, 041059 (2020).
- [11] X. Hong, M. Gillig, R. Hentrich, W. Yao, V. Kocsis, A. R. Witte, T. Schreiner, D. Baumann, N. Pérez, A. U. B. Wolter, Y. Li, B. Büchner, and C. Hess, *Phys. Rev. B* **104**, 144426 (2021).
- [12] Q. Barthélemy, E. Lefrançois, J. Baglo, P. Bourgeois-Hope, D. Chatterjee, P. Lefloïc, M. Velázquez, V. Balédent, B. Bernu, N. Doiron-Leyraud, F. Bert, P. Mendels, and L. Taillefer, *Phys. Rev. B* **107**, 054434 (2023).
- [13] Y. K. Tsui, C. A. Burns, J. Snyder, and P. Schiffer, *Phys. Rev. Lett.* **82**, 3532 (1999).
- [14] I. A. Leahy, C. A. Pocs, P. E. Siegfried, D. Graf, S.-H. Do, K.-Y. Choi, B. Normand, and M. Lee, *Phys. Rev. Lett.* **118**, 187203 (2017).
- [15] J. K. Kjems, W. Hayes, and S. H. Smith, *Phys. Rev. Lett.* **35**, 1089 (1975).
- [16] B.-Q. Liu, P. Čermák, C. Franz, C. Pfleiderer, and A. Schneidewind, *Phys. Rev. B* **98**, 174306 (2018).
- [17] P. Čermák, A. Schneidewind, B. Liu, M. M. Koza, C. Franz, R. Schönmann, O. Sobolev, and C. Pfleiderer, *Proc. Natl. Acad. Sci.* **116**, 6695 (2019).
- [18] T. Kim, K. Park, J. C. Leiner, and J.-G. Park, *Journal of the Physical Society of Japan* **88**, 081003 (2019).
- [19] M. Ozerov, N. Anand, L. J. van de Burgt, Z. Lu, J. Holleman, H. Zhou, S. McGill, and C. Beekman, *Phys. Rev. B* **105**, 165102 (2022).
- [20] C. A. Pocs, P. E. Siegfried, J. Xing, A. S. Sefat, M. Hermele, B. Normand, and M. Lee, *Phys. Rev. Res.* **3**, 043202 (2021).
- [21] J. Xing, L. D. Sanjeewa, J. Kim, G. R. Stewart, M.-H. Du, F. A. Reboredo, R. Custelcean, and A. S. Sefat, *ACS Mater. Lett.* **2**, 71 (2020).
- [22] J. Xing, L. D. Sanjeewa, J. Kim, G. R. Stewart, A. Podlesnyak, and A. S. Sefat, *Phys. Rev. B* **100**, 220407(R) (2019).
- [23] R. Bergman, *Thermal conduction in solids* (Oxford University Press, Oxford, 1979).
- [24] C. A. Pocs, I. A. Leahy, H. Zheng, G. Cao, E.-S. Choi, S.-H. Do, K.-Y. Choi, B. Normand, and M. Lee, *Phys. Rev. Res.* **2**, 013059 (2020).

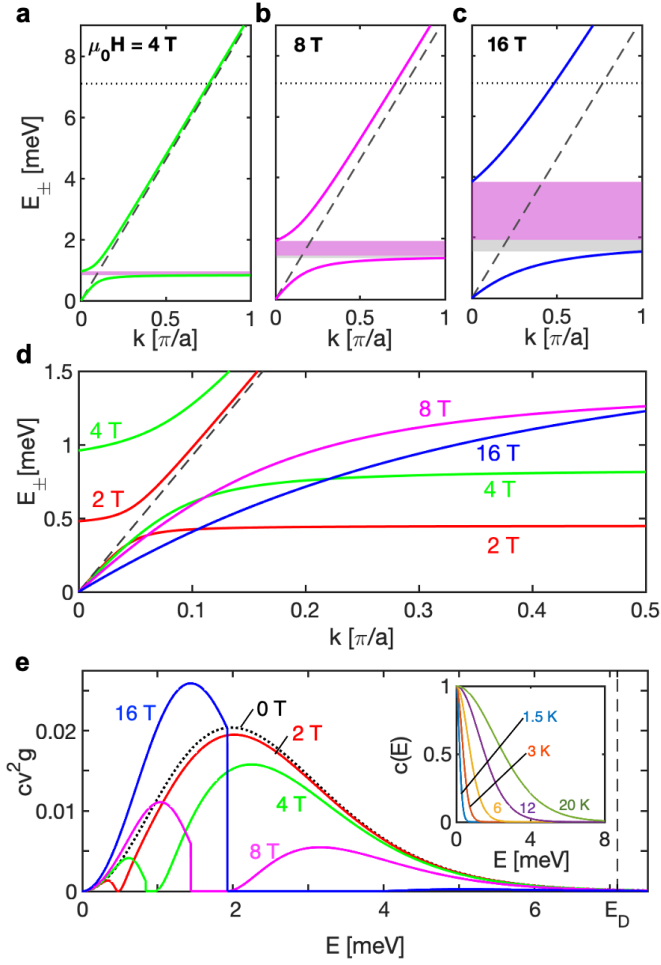


FIG. 3. **a-c**  $E_{\pm}(k)$  of Eq.(2) are plotted for  $\mu_0 H = 4, 8$  and 16 T, with  $\eta = 0.13 \text{ meV}^{-1}$  and  $a$  denoting the lattice constant. The phonon dispersion without ME coupling is shown as a dotted line, while the horizontal dashed line is the Debye energy  $E_D = 7.1 \text{ meV}$ . The energy gap ( $\Delta$ ) between upper and low branches, which is proportional to  $H^2$ , is shown with pink and gray shading. The pink shading indicates the gap including states with arbitrarily large values of  $k$ , while gray shading shows the increase in the gap upon imposing the cutoff  $k < \pi/a$ . **d**  $E_{\pm}(k)$  for several values of applied field at smaller values of  $k$ . The lower branch dispersion near  $k = 0$  moves downward in energy (*i.e.* the velocity decreases) with increasing field. **e** The integrand of Eq. (4),  $c(E)v^2(E)g(E)$ , is shown for several values of applied field at  $T = 6 \text{ K}$ . The upper and lower branches are clearly visible as two separate peaks separated by the gap, where  $g(E) = 0$ . Upon increasing  $H$ , the upper-branch contribution decreases as spectral weight moves to higher energy. Meanwhile, the contribution of the lower branch increases with field. The inset plots the specific heat  $c(E)$  at selected temperatures.

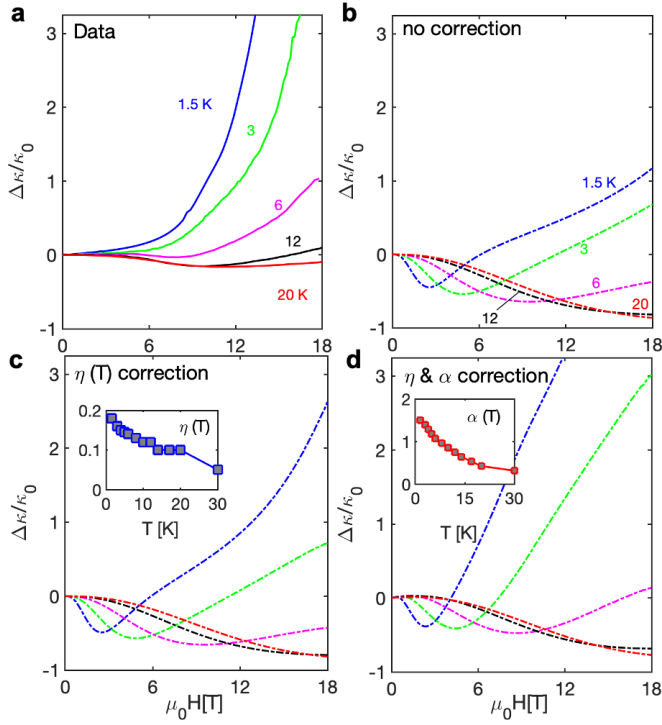


FIG. 4. **a** Comparison of measured and **b** calculated fractional thermal conductivity as a function of applied field at selected temperatures with  $\eta = 0.13 \text{ meV}^{-1}$ . **c** Calculated  $\Delta\kappa(H)/\kappa_0$  including  $T$ -dependent ME coupling strength  $\eta = \eta(T)$ , which incorporates the hard-core nature of SFEs at a mean-field level (see text and Methods).  $\eta(T)$  is chosen to optimize qualitative agreement with the data and is shown in the inset. **d** Calculated  $\Delta\kappa(H)/\kappa_0$ , including scattering of phonons by paramagnetic fluctuations estimated using the deviation from saturation of the magnetization (see text), together with  $\eta(T)$  in panel **c**. The relative strength of magnetic to non-magnetic scattering is quantified by  $\alpha$  as described in the text. The temperature-dependence of  $\alpha$  (inset) is chosen to optimize qualitative agreement with the data, where the monotonically decreasing  $\alpha(T)$  is attributed to non-magnetic phonon-phonon scattering that increases with  $T$ .